Annals of Nuclear Medicine Vol. 10, No. 4, 409–417, 1996

Abdominal SPECT/MRI fusion applied to the study of splenic and hepatic uptake of radiolabeled thrombocytes and colloids

Hanna K. POHJONEN,*[1] Sauli E. SAVOLAINEN,*[2,*3,*4] Päivi H. NIKKINEN,*[3] Veli-Pekka O. POUTANEN,*[4] E. Tapani KORPPI-TOMMOLA*[4] and B. Kristian LIEWENDAHL*[3]

*[1] *Medical Engineering Centre, Helsinki University Central Hospital,*
*[2] *Department of Physics, University of Helsinki,* *[3] *Laboratory Department, Division of Nuclear Medicine, and* *[4] *Department of Radiology, Helsinki University Central Hospital, Finland*

The importance of applying MRI (CT)/SPECT fusion in the abdominal and thoracic areas has been recognized in recent studies aiming at radionuclide therapy of cancer. According to our earlier results spleen and liver volume determination with different segmentation methods is inaccurate with SPECT alone. We therefore applied a SPECT/MRI registration procedure to the estimation of spleen and liver volumes and spleen/liver activity ratios in three male volunteers administered ^{111}In-labeled thrombocytes and ^{99m}Tc-labeled colloids. The objectives of the study were to investigate if the uptake of thrombocytes in the spleen and liver can be measured more accurately when the anatomical borders of these organs are transferred from MRI to SPECT, and to test a SPECT/MRI registration method for improving three-dimensional dosimetry for radiotherapy treatment planning. A good correlation was found between spleen/liver activity ratios calculated from volumetric average activity per pixel values and from total volumetric counts derived from registered data but not from projection data. The average registration residual with this SPECT/MRI fusion method is approximately 1–2 cm in the abdominal area. Combining anatomical images with SPECT is therefore important for improving quantitative SPECT also in the abdomen.

Key words: abdominal fusion imaging, registration, SPECT, MRI

INTRODUCTION

REGISTRATION of anatomical and functional tomographic image data has so far been applied mainly to brain studies.[1–11] The clinical benefits of adding structural information from MRI or CT to SPECT is obvious: because of the poor spatial resolution of SPECT and the lack of anatomical landmarks, regions of interest (ROIs) can be more precisely defined if anatomical information is transferred to SPECT images.[11] The importance of applying MRI (CT)/SPECT fusion in the abdominal and thoracic areas has also been recognized in recent studies aiming at radionuclide therapy of cancer.[12–16] This is because radionuclide targeting requires an accurate method for the analysis of tracer uptake as the basis for dosimetric calculations in internal radiotherapy.[12–18]

We applied our previously developed SPECT/MRI-registration procedure[11] to the estimation of spleen and liver volumes and spleen/liver activity ratios in three male volunteers administered ^{111}In-labeled thrombocytes and ^{99m}Tc-labeled colloids. The objective was to develop and test the registration method for further development of three-dimensional dosimetry for systemic radionuclide therapy applications, especially for radioimmunotherapy treatment planning. The thrombocyte spleen/liver activity ratio has diagnostic value, particularly in patients with idiopathic thrombocytopenic purpura.[19–23] Therefore another objective was to investigate if the uptake of thrombocytes in the spleen and liver can be measured more accurately when the anatomical borders of these organs are transferred from MRI to SPECT.

Received June 6, 1996, revision accepted September 18, 1996.

For reprint contact: Ms. Hanna Pohjonen, Hospital Engineer, Helsinki University Central Hospital, Medical Engineering Centre, Stenbäckinkatu 9, FIN-00290, Helsinki, FINLAND.
e-mail: hanna.pohjonen@hyks.mailnet.fi

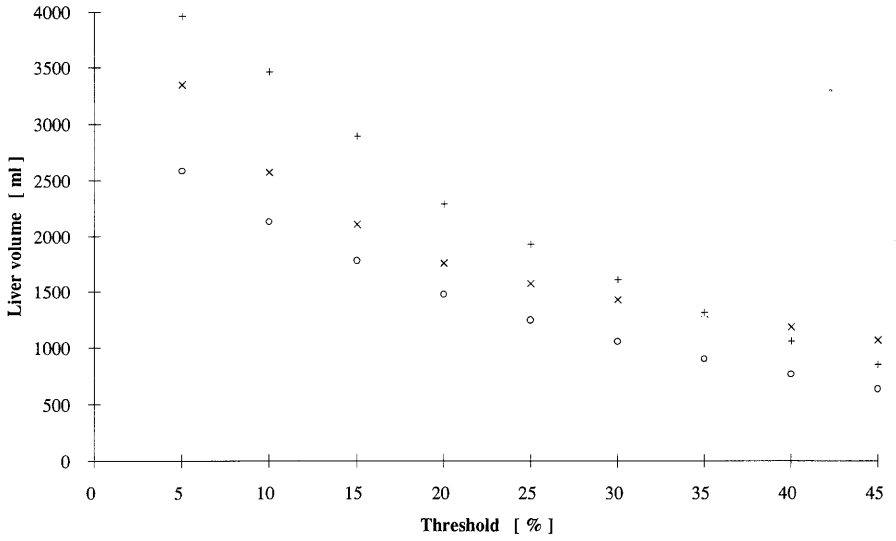

Fig. 1 Liver volume as a function of threshold in SPECT in three healthy subjects administered ^{99m}Tc-colloids (○ = volunteer 1, × = volunteer 2, + = volunteer 3).

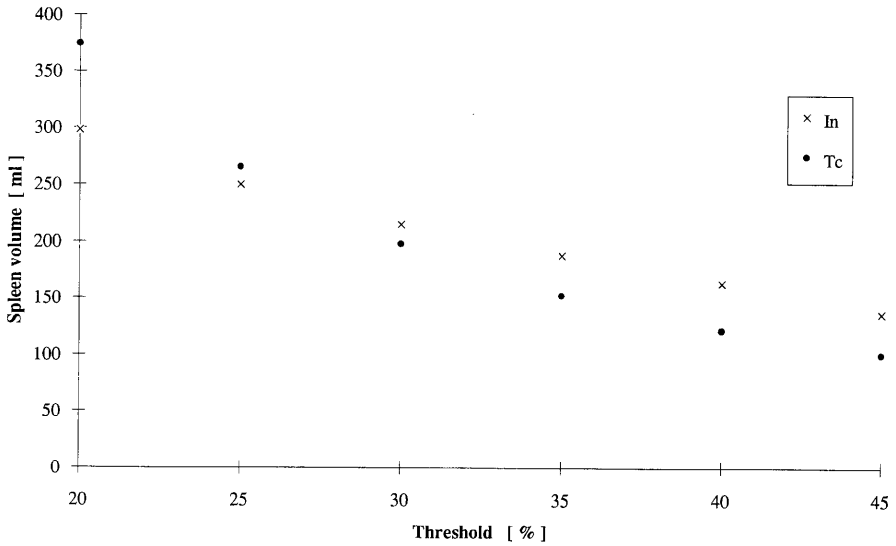

Fig. 2 Spleen volume as a function of threshold and radioisotope (volunteer 2).

MATERIALS AND METHODS

Materials. This study was approved by the local ethical committee and informed consent was obtained from all volunteers. Three healthy males volunteered for this study. Autologous thrombocytes were labeled with ^{111}In as described previously.[19] ^{99m}Tc-labeled colloids were injected two days after the study with thrombocytes.

Planar imaging. Anterior and posterior imaging (100,000 counts were collected) was performed 50 min after the intravenous injection of ^{111}In-oxine-labeled (Amersham International plc, Amersham, UK) thrombocytes (3.7–7.4 MBq). ^{99m}Tc-labeled tin colloids (Amersham International plc) (approximately 37 MBq) were injected two days later.

SPECT imaging (single, dual). SPECT imaging with a single detector camera was started about one hour after the injection. It was performed with a Picker SX300 single square detector (36 cm × 36 cm, with 0.95 cm thick Na(I)-crystal) gamma camera (Picker International, Inc., Cleveland, Ohio, USA) connected to a PDP11/74-computer with NUD-SPETS (Nuclear Diagnostics Ab, Stockholm, Sweden) software. For imaging and uptake measurement of ^{111}In-activity in the study with labeled thrombocytes a standard medium energy parallel hole collimator was used. The imaging protocol was: 64 × 64 matrix, 360°, 64 frames, 40 s per frame, and energy windows 171 keV ± 5% and 245 keV ± 10%. The counts detected in the two energy windows were summed for image processing. For the study with ^{99m}Tc-labeled colloids a low energy parallel hole collimator was used: 64 frames, 30 s per frame, and

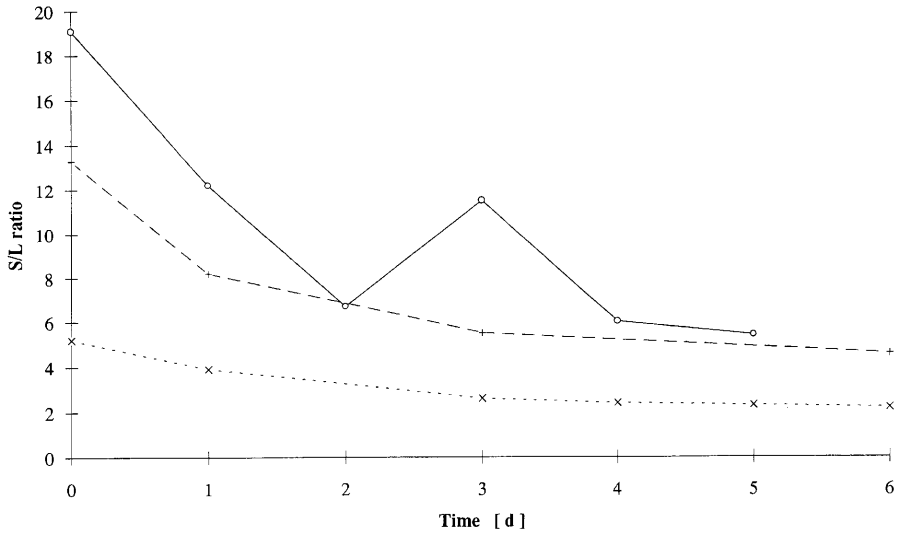

Fig. 3 Spleen/liver activity ratios derived from anterior and posterior projections (geometric mean) as a function of time in three volunteers administered ^{111}In-labeled thrombocytes (○ = volunteer 1, × = volunteer 2, + = volunteer 3).

energy window 140 keV ± 10%. Reconstruction of transversal images was performed by using the modified Shepp-Logan filter for backprojection with preattenuation correction ($\mu = 0.12$ cm^{-1} for ^{99m}Tc and $\mu = 0.07$ cm^{-1} for ^{111}In).[24-26] The pixel size and the slice thickness was 5.8 mm.

SPECT imaging with a dual detector gamma camera was performed 1–4 hours after single detector SPECT imaging. It was performed with a Picker Prism 2000 dual detector gamma camera (Picker International Inc.) equipped with medium and low energy parallel hole collimators. The imaging protocol was the same as with the single detector gamma camera except for the collection of 120 frames (30 s per image). Projection images were prefiltered with a Metz filter,[27] and transversal slices were reconstructed by applying Picker Odyssey VP software[27] from the prefiltered data by using the ramp filter. The outline of the abdominal area on transversal slices, to which a first order Chang attenuation correction was applied, was determined by asymmetric ellipse fitting. The isotope associated attenuation coefficients were 0.11 cm^{-1} for ^{99m}Tc and 0.07 cm^{-1} for ^{111}In. The pixel size and the slice thickness was 9.3 mm.

MR imaging. MR imaging was performed with a Siemens Magnetom Vision 1.5 T MRI scanner. In volunteers 1 and 2 a new high gradient performance FLASH sequence (a 600 μs risetime up to 25 mT) was used. Because acquisition times below 20 s are suitable for breathhold imaging, this T1-weighted sequence can be used with up to 19 slices. It can also take advantage of presaturations. The matrix size in this study was 128 × 128 pixels, the slice thickness 4 mm and the pixel size 3.9 mm. Volunteer 3 was examined by means of a slower MRI sequence (256 × 256 matrix, slice thickness 4 mm, pixel size 1.76 mm), which uses a gradient performance with a 600 μs risetime up to 15 mT. With this sequence it is possible to acquire only 7 slices in 20 s resulting in several breathhold periods to cover the desired area.

External markers. Four to six skin markers consisting of small plastic tubes containing a homogeneous mixture of 350 μl coconut butter and 37 kBq ^{111}In or 74 kBq ^{99m}Tc and therefore identifiable with both imaging methods were used for retrospective image registration. The external markers were positioned in the following positions: sacrum, thoracic spine, umbilicus, processus xiphoideus, and lateral margin of costa XII (2 markers). SPECT and MR imaging were performed without detaching the markers between the three studies.

Data analysis. MR and SPECT images were transferred to a Sun-5-workstation (Sun Microsystems, Inc., USA) where the mathematical transformation was computed and the registered multimodal data were visualized and analyzed. After transferring the images to the workstation, the corresponding marker positions were specified interactively on the screen. The data sets were interpolated to isotropic matrices by linear interpolation. This allows specification of marker positions performed in three dimensions. The registration algorithm follows a noniterative least squares method with a singular value decomposition of a 3 × 3 covariance matrix (see: Appendix 1).[28] After the entire transformation had been determined, MRI slices were transformed to the SPECT coordinate systems by using the nearest neighbor approximation to compute the values for the transformed voxels.

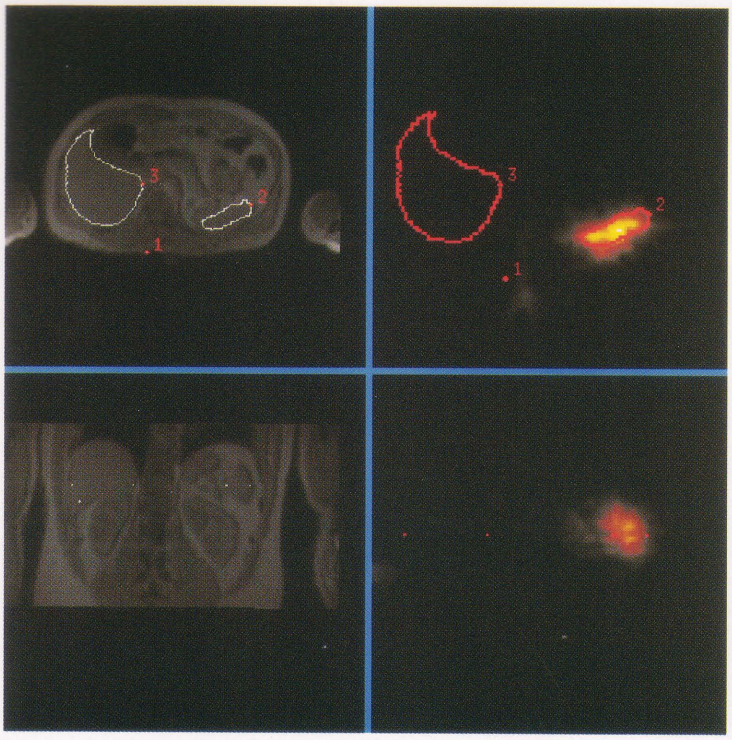

Fig. 4 Registered SPECT (^{111}In-study) and MRI data sets. Corresponding markers indicated by 1. ROIs corresponding to the spleen (2) and liver (3) have been drawn on transversal MR images. ROI positions are also shown on coronal slices. The liver is poorly visualized in SPECT because of the great difference in counts per pixel values between the liver and spleen (most thrombocytes accumulate in the spleen).

Table 1 Spleen and liver volumes determined from MRI, volumetric spleen/liver ratios based on total counts and average activity per pixel values and ratios calculated from anterior and posterior projections (geometric mean) in volunteers administered ^{111}In-labeled thrombocytes

	Camera	Liver volume (*l*)	Spleen volume (m*l*)	S/L ratio (total counts)	S/L ratio (per pixel)	S/L ratio (projection data)
Volunteer 1	single	1.66	201	0.73	6.0	19
	dual	1.69	193	0.87	7.6	
Volunteer 2	single	1.30	116	0.48	5.4	13
	dual	1.34	108	1.6	20	
Volunteer 3	single	2.38	273	0.59	5.1	5
	dual	2.43	269	2.8	25	

Table 2 Spleen and liver volumes determined from MRI, volumetric spleen/liver ratios based on total counts and average activity per pixel values and ratios calculated from anterior and posterior projections (geometric mean) in volunteers administered ^{99m}Tc-labeled colloids

	Camera	Liver volume (*l*)	Spleen volume (m*l*)	S/L ratio (total counts)	S/L ratio (per pixel)	S/L ratio (projection data)
Volunteer 1	single	1.72	198	0.15	1.3	0.7
	dual	1.73	190	0.13	1.2	
Volunteer 2	single	1.59	98	0.06	0.89	0.2
	dual	1.50	100	0.05	0.69	
Volunteer 3	single	2.89	338	0.18	1.6	0.5
	dual	2.81	326	0.15	1.3	

The spleen and liver volumes were determined from transversal SPECT images as described previously.[24,25] With the registered data sets ROIs were drawn on the transversal MR images and transferred automatically to the corresponding positions in SPECT images to calculate the number of counts in the ROIs.

RESULTS

Volume determination in non-registered SPECT. The dependence of the measured liver volumes on the selected threshold in ^{99m}Tc-SPECT is shown in Fig. 1. The liver sizes as estimated from MRI (average of four determina-

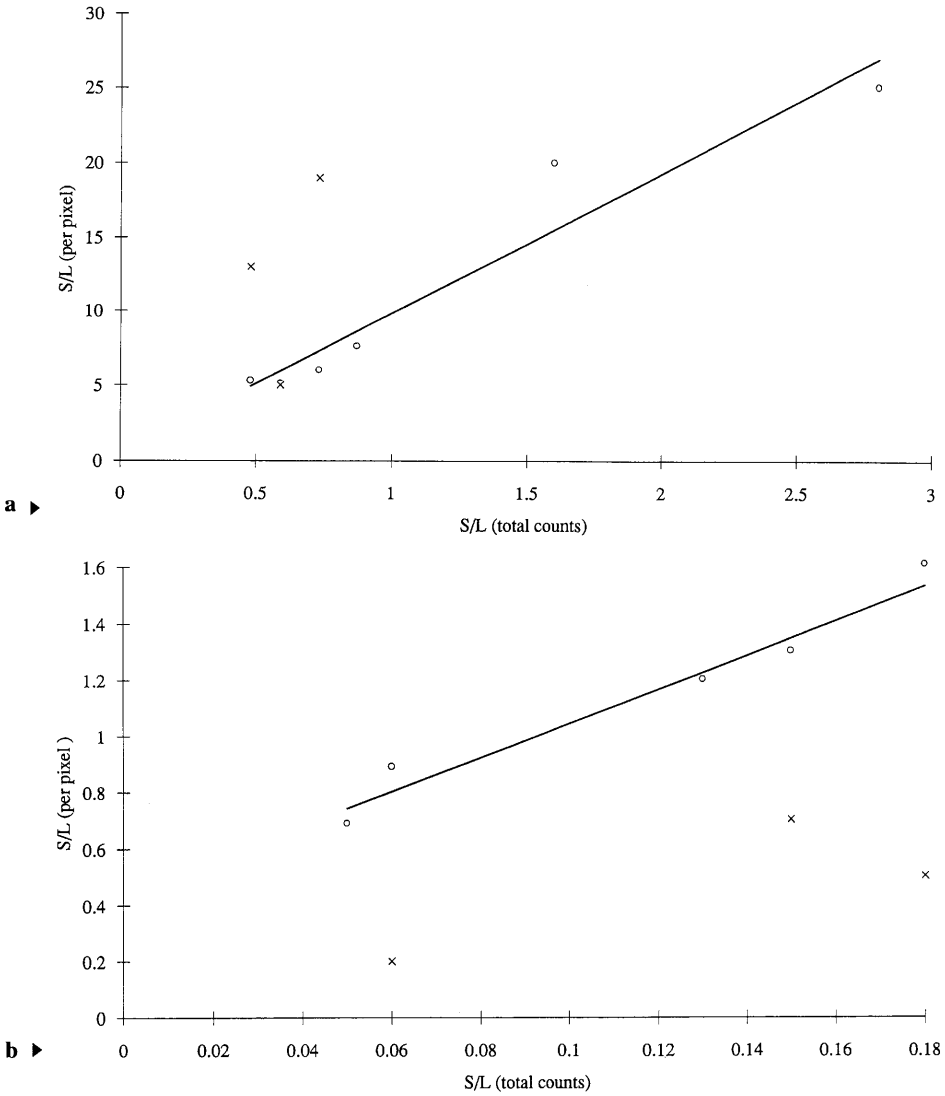

Fig. 5 Correlation between spleen/liver ratios calculated using total counts (x-axis) and average activity per pixel values (volumetric and projection data) (y-axis) a) in the ^{111}In-study and b) in the ^{99m}Tc-study (○ =volumetric per pixel values, × =projection data-based values). Regression line for volumetric values is also presented (with correlation coefficient r = 0.96 (In-study) and r = 0.98 (Tc-study)).

tions) were 1.70 l, 1.43 l, and 2.63 l for volunteers 1, 2 and 3, respectively. In Fig. 2 the spleen volume of volunteer 2 as a function of the threshold and isotope used is shown. The average spleen size determined from MRI was 106 m*l*. The single detector gamma camera was utilized for obtaining the data presented in Figs. 1 and 2.

Spleen/liver activity ratios based on projection data. Activity ratios derived from anterior and posterior projections (geometric mean) as a function of time are presented in Fig. 3. The spleen/liver activity ratio decreased remarkably during the first day after injection. There was considerable inter-individual variation in the S/L ratio and an unexpected increase at day 3 was found in volunteer 1 (which was possibly caused by a jogging exercise on that day).

Spleen and liver volumes and activity ratios based on registered SPECT and MRI. Figure 4 shows an example of the registered MRI and SPECT data sets. The anatomical borders of the spleen and liver have been drawn on the transversal MR image and transferred automatically to the corresponding positions in SPECT. The liver is poorly visualized in SPECT because of the great difference between the liver and spleen in counts per pixel values (most thrombocytes accumulate in the spleen). Despite this it is possible to determine the S/L ratio by using registered anatomical data. Information on the spleen and liver volumes determined from MR images and spleen/liver activity uptake ratios for ^{111}In-labeled thrombocytes and ^{99m}Tc-labeled colloids by using both total counts and average counts per pixel values (later referred to as volumetric per pixel values) is presented in Tables 1 and

2. For comparison, the activity ratios derived from the anterior and posterior projections (geometric mean) in the ^{111}In- and ^{99m}Tc-studies are also presented. The borders of the organs were drawn on the MRI slices by two hospital physicists.

In Fig. 5 a and b the spleen/liver activity ratios calculated by using total counts (horizontal axis) and average activity per pixel values (volumetric and projection data-based) (vertical axis) are presented. A good correlation was found between spleen/liver activity ratios calculated from volumetric average activity per pixel values and total counts derived from registered data but not from projection data.

Registration residual. The average residual mean squared (RMS) error for the registration of the SPECT and MR images from volunteers 1 and 2 (with the fast MRI sequence) was 11 mm for the single-detector gamma camera and 14 mm for the dual-detector camera. The RMS registration error in the data sets (the slower MRI sequence) in volunteer 3 was 18 mm and 15 mm, respectively. The RMS registration error in the ^{111}In-study was 11 mm in volunteers 1 and 2 and 20 mm in volunteer 3. In the ^{99m}Tc-study the RMS values were 11 mm and 14 mm, respectively.

DISCUSSION

None of the four SPECT segmentation methods previously tested by us (thresholding, grey level histogram, region growing, and combined region growing and edge detection) was found to be highly accurate for the measurement of the activity distribution of ^{111}In-thrombocytes.[25] Nevertheless, thresholding and region growing may be clinically useful, but not for dose estimation requiring great accuracy for reasons of patient safety (higher doses than in diagnostic studies). As can be seen in Figs. 1 and 2 the result is dependent on the selected threshold.

The accumulation of thrombocytes in the spleen and liver has usually been examined by conventional planar scintigraphy.[19,20,22,24,29] Van Reenen et al.[29] demonstrated that geometric mean values derived from anterior and posterior projections provide good data on quantitative regional distribution of ^{111}In-labeled thrombocytes. According to Chandler[30] SPECT is required for the measurement of the absolute uptake of ^{99m}Tc-labeled colloids, whereas for calculation of spleen/liver activity ratios planar scintigraphy is adequate. With clinically acceptable doses of radioisotopes, however, it is not possible to exactly determine the anatomical borders of the liver and spleen unless prolonged and therefore inconvenient imaging protocols are applied. Even with long acquisition times segmentation in SPECT is inaccurate and highly dependent on the segmentation methods used[25] and filtering algorithms applied.[25,31,32] Filtering also affects the amount of counts detected in ROIs. Contradictory to our earlier conclusion[24,25] and that of Chandler[30] spleen/liver activity ratios derived from projection data seem to be quite inaccurate. Registration of MRI and SPECT improves the accuracy of measurement of organ uptakes in SPECT, but in the absence of the possibility to register, it is possible to minimize the error—as shown also by Chandler[30]—by using average activity per pixel values from anterior and posterior projections in spleen/liver ratio measurements.

It is known from earlier studies that data on the kinetics of thrombocytes depend on the quantification method used and that the spleen/liver activity ratio is time dependent.[19–24,29,33–36] We observed that especially during the first day after the injection of labeled thrombocytes spleen/liver activity ratios decreased significantly as also reported by Luikens et al.,[37] who studied five control subjects, two of whom had very different spleen uptakes at 4 h and 24 h.

There have been several attempts to determine quantitative uptakes in organs by conventional planar scintigraphy and SPECT analysis.[19,20,22,24,25,29,30,37–40] Particularly in the abdomen, quantitation of SPECT is limited by inaccurate reconstruction and correction methods, such as attenuation and scatter. The filtered back-projection reconstruction process is also affected by the selected filter. There is now consensus that compensation for attenuation should be included in quantitative SPECT. There is, however, no common practice in scatter correction.[41] According to Ljungberg[42] accurate depth-dependent scatter functions are essential for proper scatter correction. We used attenuation correction that is based on an approximate assumption of uniformly distributed activity in the object.[26,41,43] Scatter was accounted for by an artificially low linear attenuation coefficient.[26,41,43] The accuracy of quantitation achieved in ^{99m}Tc-imaging cannot be expected in ^{111}In-imaging and therefore most studies on SPECT quantitation have been performed with ^{99m}Tc.

The registration accuracy of brain SPECT, with a single detector gamma camera, and MRI yield results of 3–4 mm with our registration method.[44] The use of more than six markers did not significantly increase the accuracy of registration. In this work, the registration error was determined as the RMS error of the fitting of the marker point sets. This is the remaining residual not explained by the transformation matrix. It does not tell about the actual registration accuracy, but tells about the success of fitting the corresponding markers specified by the user. An accuracy of approximately 1–2 cm, derived in this work, is usually sufficient in abdominal fusion imaging, but can be improved by using bigger matrix sizes and smaller pixel sizes in SPECT. The finite pixel size is the basic error always present in fitting two marker sets. On the other hand, for reasons of statistics, it is not convenient to use very large matrix sizes. In this study, the pixel sizes were larger in dual detector SPECT, resulting in larger

registration errors as well. On the other hand, imaging time was reduced with the dual detector camera.

Volunteers 1 and 2 were examined by using a new MRI sequence enabling fast recording during breathholding. This is a very important improvement in registration, because it results in fewer separate slice stacks in the study and better registration accuracy. It is very difficult to hold the breath repeatedly in the same way during imaging of every stack, leading to incontinuities at the borders of the stacks. The slight difference in the volume estimates of the spleen and liver is probably caused by inaccuracy in determining organ boundaries due to breathing during MR imaging. However, CT and spiral CT can be used for liver imaging with one shot. This would increase registration accuracy, but also the radiation dose to the patient.

There are several other factors influencing registration error in abdominal fusion imaging including breathing, movement of the markers and non-rigidness of the body as compared to the skull. The human head is a relatively stable object and global rigid matching suffices for matching brain images obtained by different methods. Deformable body parts, such as the abdomen, may need local transformations with higher elasticity. Matching of objects that change shape between scans or move when being studied need to be evaluated carefully. On the other hand, global affine transformation has been successfully applied to register CT and SPECT in abdominal studies.[13] We used external markers for registration because of the difficulty of extracting anatomical surfaces from SPECT images due to the functional nature of SPECT. For more accurate calculation of the transformation matrix it would be desirable to have more than 4–6 points in the fitting, as this could partly compensate for potential errors.

In conclusion, we describe a fast noniterative method for abdominal SPECT/MRI fusion imaging employing external markers. A good correlation was found between spleen/liver activity ratios calculated from volumetric average activity per pixel values and total counts derived from registered data but not from projection data. Combining anatomical images with SPECT is important for improving quantitative SPECT in the abdomen. This procedure can be directly applied to the registration of SPECT and CT images as well, and it will be part of a software package for calculating individual 3D-dosimetry by using e.g. MIRD-formalism.

ACKNOWLEDGMENTS

This work was supported by grants from the Finnish Society of Nuclear Medicine, Emil Aaltonen's Foundation and Oskar Öflund's Foundation.

APPENDIX 1

The registration algorithm is based on a noniterative least squares method utilizing a singular value decomposition (SVD) of a 3×3 covariance matrix.[28] The marker point sets $\{p_i\}$ and $\{p_i^*\}$, $i = 1, 2, \ldots, N$ (altogether N markers), are related by

$$p_i^* = S_c(Rp_i) + T. \quad (1)$$

Here R is a rotation matrix, T a translation vector and S_c a scaling factor which is known from phantom measurements. The least squares solution for R and T is found by minimizing the error sum

$$S^2 = \sum_{i=1}^{N} \| p_i^* - (Rp_i + T) \|^2. \quad (2)$$

It is possible to decouple the rotation and translation components by subtracting the centroid coordinates from the marker coordinates to get the marker point sets q_i and q_i^* relative to the centroids c and c^*. The rotation matrix can therefore be calculated by minimizing the sum

$$S^2 = \sum_{i=1}^{N} \| q_i^* - Rq_i \|^2. \quad (3)$$

In order to find the least squares solution for R an SVD of the following 3×3 covariance matrix H is computed (q' = the transpose of q)

$$H = \sum_{i=1}^{N} \| q_i q_i^{*\prime} = U\Omega V'. \quad (4)$$

The 3×3 matrices U and V are orthonormal, and Ω is a 3×3 diagonal matrix where the elements are positive. The rotation matrix R equals X

$$X = VU', \quad (5)$$

if the determinant of X is + 1. The translation matrix T is now given by

$$T = c^* - Rc. \quad (6)$$

REFERENCES

1. Bohm C, Creitz T, Kingsley D, Berggren BM, Olsson L. Adjustable computerized stereotaxic brain atlas for transmission and emission tomography. *Am J Neuroradiol* 4: 731–733, 1983.
2. Hawkes DJ, Hill DLG, Lehmann ED, Robinson GP, Maisey MN, Colchester ACF. Preliminary work on the interpretation of SPECT images with the aid of registered MR images and an MR derived 3D neuro-anatomical atlas. *In* NATO ASI Series, 3D imaging in medicine, KH Hohne, et al. (eds.), Berlin, Heidelberg, New York, Springer-Verlag, pp. 241–251, 1990.
3. Bergström M, Boëthius J, Eriksson L, Greitz T, Ribbe T, Widén L. Head fixation device for reproducible position alignment in transmission CT and positron emission

tomography. *J Comp Ass Tomog* 5: 136–141, 1981.
4. Fox PT, Perlmutter JS, Raichle ME. A stereotactic method of anatomical localization for positron emission tomography. *J Comp Ass Tomog* 9: 141–153, 1985.
5. Mazziotta JC, Phelps ME, Meadors AK, Ricci A, Winter J, Bentson JR. Anatomical localization schemes for use in positron computed tomography using a specially designed headholder. *J Comp Ass Tomog* 6: 848–853, 1982.
6. Miura S, Kanno I, Iida H, et al. Anatomical adjustments in brain positron emission tomography using CT images. *J Comp Ass Tomog* 12: 363–367, 1988.
7. Pelizzari CA, Chen GTY, Spelbring DR, Weichselbaum RR, Chen CT. Accurate three-dimensional registration of CT, PET, and/or MR images of the brain. *J Comp Ass Tomog* 13: 20–26, 1989.
8. Schiers C, Tiede U, Höhne KH. Interactive 3D registration of image volumes from different sources. *In* Proceedings of CAR'89 Computer Assisted Radiology, Lemke HU, Rhodes ML, Jaffe CC, Felix R (eds.), Berlin, Springer-Verlag, pp. 666–670, 1989.
9. Hill DLG, Hawkes DJ, Crossman JE, et al. Registration of MR and CT images for skull base surgery using point-like anatomical features. *Brit J Radiol* 64: 1030–1035, 1991.
10. Spetsieris PG, Dhawan V, Takikawa S, Margouleff D, Eidelberg D. Imaging cerebral function. *IEEE Comput Graph Appl* 13: 15–26, 1993.
11. Pohjonen H, Nikkinen P, Sipilä O, et al. Registration and display of brain SPECT and MRI using external markers. *Neuroradiology* 38: 108–114, 1996.
12. Sgouros G, Chiu S, Pentlow KS, et al. Three-dimensional dosimetry for radioimmunotherapy treatment planning. *J Nucl Med* 34: 1595–1601, 1993.
13. Kramer E, Noz ME, Sanger JJ, Megibow AJ, Maguire GQ. CT-SPECT fusion to correlate radiolabeled monoclonal antibody uptake with abdominal CT findings. *Radiology* 172: 861–865, 1989.
14. Birnbaum BA, Noz ME, Chapnick J, et al. Hepatic hemangiomas: diagnosis with fusion of MR, CT, and Tc-99m-labeled red blood cell SPECT images. *Radiology* 181: 469–474, 1991.
15. Koral KF, Zasadny KR, Kessler ML, et al. CT-SPECT fusion plus conjugate views for determining dosimetry in iodine-131-monoclonal antibody therapy of lymphoma patients. *J Nucl Med* 35: 1714–1720, 1994.
16. Tjuvajev JG, Homer AM, Daghighian F, et al. Imaging of brain tumor proliferative activity with iodine-131-iodo-deoxyuridine. *J Nucl Med* 35: 1407–1417, 1994.
17. Strand S-E, Zanzonico P, Johnson TK. Pharmacokinetic modeling. *Med Phys* 20: 515–527, 1993.
18. Leichner PK, Koral KF, Jaszczak RJ, Green AJ, Chen GTY, Roeske JC. An overview of imaging techniques and physical aspects of treatment planning in radioimmunotherapy. *Med Phys* 20 (2): 569–578, 1993.
19. Syrjälä MT, Savolainen S, Nieminen U, Gripenberg J, Liewendahl K, Ikkala E. Splenic dynamics of indium-111 labeled platelets in idiopathic thrombocytopenic purpura. *J Nucl Med* 30: 1546–1549, 1989.
20. Siegel RS, Rae JL, Barth S, et al. Platelet survival and turnover: important factors in predicting response to splenectomy in immune thrombocytopenic purpura. *Am J Hematol* 30: 206–212, 1989.
21. Najean Y, Ardaillou N. The sequestration site of platelets in idiopathic thrombocytopenic purpura: its correlation with the results of splenectomy. *Br J Haematol* 21: 153–164, 1971.
22. Stratton JR, Ballem PJ, Gernsheimer'T, Cerqueira M, Slichter SJ. Platelet destruction in autoimmune thrombocytopenic purpura: kinetics and clearance of ^{111}In-labelled autologous platelets. *J Nucl Med* 30: 620–637, 1989.
23. Savolainen S, Liewendahl K, Syrjälä MT, Gripenberg J. Platelet splenic transit times in idiopathic thrombocytopenic purpura: Compartmental vs. non-compartmental model. *Int J Hematol* 55: 81–87, 1992.
24. Savolainen S. SPECT versus planar scintigraphy for quantification of splenic sequestration of ^{111}In-labelled platelets. *Nucl Med Commun* 13: 757–763, 1992.
25. Savolainen S, Pohjonen H, Sipilä O, Liewendahl K. Segmentation methods for volume determination with ^{111}In/^{99}Tc^{m} SPET. *Nucl Med Commun* 16: 370–377, 1995.
26. Larsson SA. Gamma camera emission tomography. *Acta Radiol* Suppl. No. 363, 1980.
27. Picker Nuclear Medical Imaging Systems. Odyssey VP Operator's guide, Ohio, Picker International, Inc., Ohio Imaging Division, Bedford Heights, 1995.
28. Arun KS, Huang TS, Blostein SD. Least-squares fitting of two 3-D point sets. *IEEE Trans Patt Anal Mach Intell* PAMI-9: 698–700, 1987.
29. van Reenen O, Lötter MG, Heyns A du P, et al. Quantification of the distribution of ^{111}In-labelled platelets in organs. *Eur J Nucl Med* 7: 80–84, 1982.
30. Chandler ST. A comparison of liver-spleen ratios and uptakes obtained using planar and tomographic techniques. *Nucl Med Commun* 10: 297–307, 1989.
31. Long DT, King MA, Sheehan J. Comparative evaluation of image segmentation methods for volume quantitation in SPECT. *Med Phys* 19 (2): 483–489, 1992.
32. Savolainen SE, Liewendahl BK. Analysis of scintigrams by singular value decomposition (SVD) technique. *Ann Nucl Med* 8 (2): 101–108, 1994.
33. Aster RH. Pooling of platelets in the spleen: role in the pathogenesis of "hypersplenic" thrombocytopenia. *J Clin Invest* 45: 645–657, 1966.
34. Kernoff LM, Blake KCH, Shackleton D. Influence of the amount of platelet-bound IgG on platelet survival and site of sequestration in autoimmune thrombocytopenia. *Blood* 55: 730–733, 1980.
35. Mueller-Eckhardt C, Mueller-Eckhardt G, Kayser W, Voss RM, Wagner J, Kuenzelen E. Platelet associated IgG, platelet survival, and platelet sequestration in thrombocytopenic states. *Br J Haematol* 52: 49–58, 1982.
36. Peters AM, Lavender JP. Factors controlling the intrasplenic transit of platelets. *Eur J Clin Invest* 12: 191–195, 1982.
37. Luikens B, Forstrom LA, Johnson T, Johnson G. Indium-111 platelet kinetics in patients with diabetes mellitus. *Nucl Med Commun* 9: 223–234, 1988.
38. Fleming JS. A technique for the absolute measurement of activity using a gamma camera and computer. *Phys Med Biol* 24: 176–180, 1979.
39. Strauss LG, Clorius JH, Frank T, van Kaick G. Single photon emission computerized tomography (SPECT) for estimates of liver and spleen volume. *J Nucl Med* 25: 81–85, 1984.

40. van Rensburg AJ, Lötter MG, Heyns A du P, Minnaar PC. An evaluation of four methods of ^{111}In planar image quantification. *Med Phys* 15: 853–861, 1988.
41. Yanch JC, Flower MA, Webb S. Improved quantification of radionuclide uptake using deconvolution and windowed subtraction techniques for scatter compensation in single photon emission computed tomography. *Med Phys* 17: 1011–1022, 1990.
42. Ljungberg M. Development and evaluation of attenuation and scatter correction techniques for SPECT using the Monte Carlo method. Doctoral Dissertation, Department of Radiation Physics, University of Lund, Klippan, Sweden, Ljungbergs Tryckeri AB, 1990.
43. Harris CC, Greer KL, Jaszczak RJ, Floyd CE Jr, Fearnow EC, Coleman RE. Tc-99m attenuation coefficient in water-filled phantoms determined with gamma cameras. *Med Phys* 11: 681–685, 1984.
44. Sipilä O, Nikkinen P, Pohjonen H, Poutanen V-P, Karp P, Liewendahl K. Evaluation of registration error in ^{99m}Tc-HM-PAO brain SPET and MRI. *In* European Association of Nuclear Medicine Congress, Brussels, Belgium, 1995. *Eur J Nucl Med* 22: 767 (Abstract 169), 1995.